# Final Report for

# Switch-Scan Linear X-ray Source

# Phase I SBIR Project

January 4, 1995

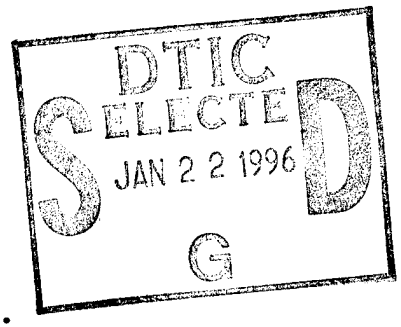


Contractor: Bio-Imaging Research, Inc.
425 Barclay Boulevard
Lincolnshire, IL 60069

Contract No.: DAAE30-95-C-0027

Project dates: March 15 to December 21, 1995

Key Person: John F. Moore, Ph.D.

# Contents

# Summary

The final goal of this project is to produce a novel x-ray generator for use in a high-speed scanner for cargo inspection. The speed requirement is too fast to allow mechanical rotation of a conventional x-ray tube. Instead, the x-ray source position must be moved by electrical means within a stationary generator. Our approach generates x-ray photons from electrons that hit a moving spot on a long anode.

In this Phase I project, we successfully demonstrated a practical method to produce such a linear scanning x-ray source. Our experimental data confirm that we can exceed the requirements for current density, source size, and switching speed. Specifically, we achieved the following goals:

Design goals (see Studies, below).

- We defined a suitable x-ray source configuration, using multiple gridded cathodes and a common anode. Each cathode-grid assembly illuminates a spot on the anode that produces a discrete x-ray source. The control grid for each cathode allows independent switching of each individual x-ray source. With a linear array of cathodes and a straight anode, we obtain a linear array of discrete sources. Other geometries could be used to obtain, for example, a rectangular grid of sources or a curved one-dimensional array. This configuration was chosen after a meeting at Picatinny to review overall system requirements, where the decision was made not to use beam deflection. The original proposal had suggested deflection electrodes that would add a continuous linear sweep to the discrete cathode switching. While that is possible for other applications, it was decided to concentrate this program's efforts on a sequence of fixed spots. With discrete cathode-grid assemblies defining the set of x-ray source spots, the overall dimensions of the tube can be reduced greatly, compared with a deflected-beam system. Also, the spots can be activated in arbitrary order, and more than one spot can be active at once, if desired. The final design parameters are listed in System studies, below.

- We carefully considered the optimum parameters for the vacuum-tube triode formed by such a cathode, its associated grid, and the common anode. Specifically, we determined the amplification factor and perveance values that give high current at negative grid voltage, but allow efficient switching of the beam current with low switching voltages.

- We designed a simple, low-cost solid-state switching circuit to switch individual cathodes on and off at sub-microsecond switching speeds. Practical pulse widths range from about 10 $\mu$s up to seconds.

- A number of physical problems in the tube structure were investigated and solved, including anode bending due to differential temperatures and alternation in spot position.

Experiments (see Experimantal Tests, below).

- We rebuilt our laboratory vacuum system with a new pump to obtain a sufficiently low pressure to operate the cathodes.

- We repaired our existing anode assembly and installed it in the vacuum chamber, to test the vacuum-tube parameters of the system and generate x-rays from electron current.

- We installed different configurations of cathode-grid assemblies to verify cathode switching and cathode current capabilities.

- We verified the emission characteristics of the dispenser cathodes and developed a procedure to activate the cathodes.

- We measured the vacuum-tube parameters of the triode formed by the cathode-grid assembly and the anode, and verified that we can easily obtain sufficient cathode current for the application with low control voltages applied to the grid.

- We built, tested, and installed the external circuitry to switch the cathode current. We verified the current accuracy and switching speed of the board at both low and high currents. The high currents were considerably higher than required by Picatinny's application.

- Using the switching circuit, we successfully pulsed actual cathode-grid assemblies, single and multiple, and obtained fast rise and fall times on short and long pulses. We successfully operated multiple cathodes at the duty cycle required by the application and at higher duty cycles.

- We demonstrated x-ray emission from single and multiple cathodes, obtaining multiple x-ray source spots on the anode that corresponded to the design. The spot sizes were verified using a pinhole camera.

## Studies

System studies.

All program participants met at Picatinny on March 21, 1995 to review overall systems concepts, source parameters, detectors, and other aspects of the system. A significant result of the analysis was a clear indication that a continuously swept beam will not give the performance required, while a series of successively illuminated x-ray source spots will. Though this obviated previous work on accelerating electrodes, deflecting electrodes, and drift space, it has the advantage of leading to a substantially simpler and lower-cost system. Our request that the scope of work be modified to confirm the changes in concept was granted.

The parameters believed to be needed for the application are listed below. Where a range is given, it does not mean that the parameter is variable, bur rather that we are not aware of what the final value of the parameter will be.

System parameters.

| | |
|---|---|
| • Object Speed | 61 cm/s (24 in/s) |
| • Slice Thickness or Spacing | 1 cm (0.39") |
| • Scan Time | 16.4 ms/slice |
| • Aperture Size: | 120 to 130 cm (47 to 51") |
| • Number of Source Spots: | 32 to 96 |
| • Sources per Side: | 8 to 24 |
| • Source Spot Spacing: | 5 to 16.3 cm (1.97" to 6.42") |
| • "On" Time per Spot: | 0.68 to 2.05 ms |
| • Duty Factor per Spot: | 4.2% to 12.5% |
| • Spot Diameter: | 1 to 3 mm (0.04 to 0.12") |
| • Cathode current: | 5 to 10 mA |
| • Anode voltage: | 120 to 160 kV |

The source geometry will be as follows:

- Linear on two sides, "Roof" shape on top;
- Sources staggered in direction of travel so that the top source and both sides can emit simultaneously.

Cathode parameters for the successive spot approach were defined, and four cathodes of different diameters were ordered for the Phase I experiments.

We studied the photon-counting rates that could be achieved at the detectors' maximum counting rate (5 million/sec). The purpose was to estimate the number of photons per sample in each of five energy bands. The results of this study are tabulated in Table 1.

Tube design studies.

The original configuration was to have two rows of cathodes: the even-numbered ones on the right and the odd-numbered ones on the left. This permits greater center-to-center cathode spacing in each row, for a given spot spacing on the anode. However, it means that the even-numbered spots on the anode will be slightly offset from the odd-numbered spots. Our present design for cathode-grid assemblies allows them to be built on 15 mm (0.59")

centers, which obviates the need for two cathode rows. For other applications, a comb collimator can be used to obtain discrete spots on a plane spaced away from the x-ray tube anode.

Anode design studies.

Electrons hit only one side of the anode, heating the front more than the back. This causes the front to expand more than the back, and the long anode will bow. In the original design, with a 12.7 mm-thick (0.5") hollow linear anode, a temperature differential of 100° C (180° F) would cause excessive bowing: 27.6 mm (1.09") for a 1.3 meter (51") length, or 6.9 mm (0.27") for half that length. Therefore, we redesigned the anode for a thicker cross section, to provide a better heat conduction path from front to back (reducing the temperature differential) and to increase the section stiffness. The new estimated bowing is 5.2 mm (0.2") for the longer length and 1.3 mm (0.05") for the shorter. These values are a small enough fraction of the cathode-to-anode spacing to be acceptable. We checked these calculations experimentally, as described later.

The maximum anode bending can be calculated by assuming different temperatures on opposite sides of a simple, flexible object of length $x$ with a rectangular cross-section. This geometry is illustrated in Figure 1. In that case, the differential expansion (in length) of the hotter side will be

$$\Delta x = xc\Delta T$$

where $\Delta T$ is the difference in temperature between the two sides and $c$ is the thermal coefficient of expansion of the material. By simple geometry, the bent arc will subtend an angle

$$\theta = \Delta x/t \quad ,$$

where $t$ is the thickness of the rectangle between the two sides with differing temperatures; the radius of the arc will be

$$r = x/\theta \quad .$$

The deviation from a straight line will be

$$D = r - r\cos(\theta/2) \simeq x^2 c\Delta T/(8t)$$

for small angles.

If the anode is stiff, the bending will be less, with the creation of internal strain. With this in mind, we designed the anode with a thin section on the front (heated) side and a thick section elsewhere. This had the additional advantage of good thermal conductivity from front to back. Since the actual cross-section was too complicated to calculate, we performed an experimental test, described later.

Cathode choice.

This system uses thermionic emission of electrons from discrete cathodes. Based on our previous experience with switched-cathode sources, we chose "dispenser" cathodes, which use a tungsten matrix impregnated with a barium compound. In operation, an elemental barium layer forms at the cathode surface, replenished by reduction of barium compounds diffusing from the interior of the hot cathode. This barium layer has a much lower work function than tungsten, and allows thermionic emission at much lower temperatures than tungsten, but the tungsten structure allows the barium surface to work at a relatively high temperature for barium. Normal operating temperatures are between 1000 and 1100° C. These cathodes were originally developed for use in spacecraft vacuum tubes, and have a proven history of long lifetimes. They are commercially available; we obtained these devices from SpectraMat, Inc. in California. In the time available for this Phase I study, we concentrated on 0.200" (5 mm) diameter cathodes, since the measured currents can be scaled easily to other cathode areas.

Tube parameter studies.

One study gave us surprising results, which were borne out by experiment. We analyzed the fundamental vacuum-tube equations to determine the best choice of vacuum-tube parameters for this application. X-ray tube operation (with almost constant anode-cathode voltage) differs from conventional triode vacuum tube

circuits, which operate normally with a substantial load impedance in series with the anode to amplify the signal applied to the grid. In our case, we do not attempt to "swing" the anode voltage, only the cathode-anode current. We defined the following important requirements for our vacuum tube:

- To minimize the cost of the external switching circuit, we need a small "grid base", the difference between the grid-cathode voltage at cut-off (zero cathode current) and at the operating current. As a practical matter, a grid base less than about 200 V allows the use of low-cost solid-state devices.

- If the grid-cathode voltage is positive, then a fraction of the cathode current will flow to the grid. This will heat the grid and reduce the useful flow of electrons to the anode. Therefore, the grid-cathode voltage at the operating current should be negative. This implies that the cathode current at zero grid-cathode voltage should be higher than the operating current.

- However, we are not concerned directly about the actual value of the cut-off grid-cathode voltage, so long as the previous two conditions are met. Our switch circuit can produce a finite peak-to-peak voltage at the cathode terminal (with respect to ground), and we can vary the DC voltage at the grid terminal (again, with respect to ground) at will, so that the swing of grid-cathode voltage covers the needed range. With negative-definite grid-cathode voltage, the DC supply for the grid bias does not supply any power, since the grid current will be negligible.

Given these requirements, we analyzed the fundamental triode equations to see how we could minimize the grid base and keep the grid-cathode voltage negative at the operating current. First, we examined the fundamental equations for the space-charge limited triode. When the cathode current is space-charge limited, it is independent of the cathode temperature (so long as the cathode is hot enough to supply more electrons than the space charge will allow), and therefore the operation is more stable than in the emission-saturated regime. The analysis described below uses approximate space-charge equations to simplify the discussion, but our detailed analysis of the more exact equations gave virtually the same results.

The space-charge limited triode is described by two important parameters:

- triode perveance $G$
- amplification factor $\mu$

The approximate equation for the cathode current $I_k$ as a function of the anode-cathode voltage $V_a$, the grid-cathode voltage $V_c$, and these parameters is

$$I_k = G \times (V_c + V_a/\mu)^n \quad ,$$

where the exponent $n$ is approximately 3/2. From this equation, we immediately see that the cut-off voltage is given by

$$V_{co} = -V_a/\mu \quad ,$$

which might suggest that a high value of $\mu$ is desirable. However, the zero-bias current is given by

$$I_z = (V_a/\mu)^n \quad ,$$

so a high value of $\mu$ will limit this current and may require a positive grid bias to obtain the desired operating current. When the equation for $I_k$ is solved for the two grid voltage values (cut-off and operating) that define the grid base, we obtain

$$\Delta V_c = V_I - V_{co} = (I/G)^{1/n} \quad ,$$

which is <u>independent</u> of $\mu$, but depends on the operating current $I$ and the perveance $G$. A more exact analysis gives

$$\Delta V_c \propto \mu/(\mu+1) \quad ,$$

which is almost independent of $\mu$ when $\mu > 100$. Finally, the operating grid voltage is

$$V_I = V_{co} + (I/G)^{1/n} = -V_a/\mu + (I/G)^{1/n}$$

Within limits, we can change the perveance and amplification

factor independently, by changing the triode geometry. From these equations, we see that only the perveance affects the grid base, which determines the switching voltage, but that both the perveance and the amplification factor determine the grid voltage at the operating current, which we want to keep negative. To obtain a small grid base, we must keep the perveance high. To operate at negative grid voltages, we must not use too high an amplification factor. The latter observation was contrary to our initial expectation and to conventional wisdom.

Now, the perveance and amplification factor depend on the following dimensions:

- anode-grid spacing
- cathode-grid spacing
- grid geometry
- effective cathode area

In general, this dependence is complicated, but we can make these simple generalizations (strictly true for parallel plane electrodes):

- The amplification factor $\mu$ depends on the grid geometry (wire size and spacing), and on the spacing between the grid and anode. It does not depend on the grid-cathode spacing.

- The perveance $G$ is proportional to the cathode area $A_k$, so we may scale our data to other geometries by this area (or use the cathode current areal density as our variable). It also depends inversely on the product of the grid-cathode and grid-anode spacings $d_{gk}$ and $d_{ga}$. It does not depend on the grid geometry. That is,

$$G \propto A_k/(d_{gk} \times d_{ga}) \quad .$$

The anode-grid spacing is determined by the required anode voltage (to avoid breakdown). We therefore must keep the cathode-grid spacing as small as practicable, to obtain a high perveance. However, a tight grid (small space between wires) gives a high amplification factor, which limits the zero-bias current. Using experimental data from our earlier project, we decided to use a very small grid-cathode spacing (0.026" = 0.66 mm), but to use a looser grid than before (40 lines per inch

instead of 60). From the earlier data, we expected $\mu$ to be about 700 to 800, and our experimental data agreed with those empirical values.

## Experimental Tests

### Experimental tube construction

To prove the concept of the switched-cathode x-ray tube in this Phase I project, we used an existing experimental vacuum chamber with a high-voltage feedthrough capable of 85 kV operation. The long cylindrical anode mounts along the chamber axis. Different cathode assemblies connect to external circuits through a multiple-pin electrical feedthrough. The experimental vacuum tube is sketched in Figure 2. Here are the important dimensions for the experimental tube structure:

- Anode diameter = 35 mm (1.38")
- Anode-grid spacing = 35 mm
- Cathode-grid spacing = 0.66 mm (0.026")
- Cathode diameter = 5 mm (0.20")
- Grid geometry: 125 $\mu$m wires on 635 $\mu$m square grid
  (40 lpi mesh of 0.005" foil)

The cathodes were SpectraMat STD-200 dispenser cathodes. Each is a 0.20" (5 mm) diameter cylinder with an impregnated disk at the end to emit electrons. Each cathode has a resistive heater potted inside the cylinder to heat the entire cylinder to the operating temperature. Because of the high temperatures, we used molybdenum for the metal pieces in the cathode assembly and high-purity alumina for the ceramic insulators, to the extent possible.

### X-ray source sequencing and control.

The cathode sequence discussed in "Designs" has been operated successfully. We fabricated and tested the feedback-controlled

constant-current cathode switch circuit and built several PC boards for the experimental work.

Cathode pulsing experiments.

The experimental work reported here was performed with 5 mm diameter cathodes. The current can be scaled (by the area of the cathode) to different values. Using the cathode switch boards, we could switch the cathode current on and off with modest voltages, less than 200 V peak-to-peak, which are easily obtained with conventional power semiconductors. Our switch circuit uses off-the-shelf N-channel MOSFETs; no high-voltage switching vacuum tubes were required. Rise and fall times of the cathode current were measured to be less than 1 microsecond, typically 200 to 800 nsec, depending on the bias level of the switching circuit. In the experimental tests described below, we controlled the pulse timing with laboratory pulse generators, using pulse widths between 10 $\mu$s and 1 ms. We tested and calibrated the switching boards on the bench, before connecting to the experimental tube.

In our first tests, we installed a single cathode-grid assembly without the anode; these two electrodes formed a vacuum diode. With the diode, we determined the operating temperature requirements and the cathode activation procedure to achieve the required cathode emission. We could obtain the required cathode current at modest cathode temperatures, approximately 1025° C. At this low temperature, cathode life should be greater than 100,000 hours, according to the manufacturer.

In the second tests, we added the anode and high-voltage supply to the single cathode and grid to make a triode. Then, we used our solid-state switching board to pulse the current, and we measured the cathode current *vs.* anode and grid voltages, and the rise and fall times of the current pulses.

Based on those results, we improved the design of the grid assembly to increase the anode voltage capability. We then installed two cathodes with the improved grid frames to test multiple-cathode operation. With two cathode-grid assemblies, we applied a two-phase pulse train to the two cathode switch boards, to pulse one cathode after the other. In these tests, we obtained pulses up to 100 mA (current limited by the setting of

the switch board) at anode voltages up to 80 kV. The actual current requirement for this system is less than 10 mA. With this triode structure, we were able to obtain this current with large negative grid-cathode voltages, as desired. Specifically, we obtained 100 mA of cathode current with 80 kV anode voltage and a grid-cathode voltage of -45 to -60 V.

We measured the vacuum-tube parameters of our experimental system for anode voltages up to 80 kV. These data are graphed in Figure 3 (cathode current *vs.* anode and grid voltage) and Figure 4 (cutoff grid voltage *vs.* anode voltage). Analyzing the data, we obtained $\mu$ values of 770 and 835 for the two triodes, at $I_k$ = 60 mA and $V_A$ = 75 kV. Extrapolating the measured cut-off voltages to $V_A$ = 160 kV, we obtain cut-off grid voltages of -300 and -350 V; at the low current densities required for this work, the operating grid bias would be about about -100 to -150 V, so the grid base is still less than 200 V.

We also verified that we could operate the cathodes continuously at the required duty factor. In these tests, we operated each cathode at a narrow pulse width, with a short delay between the first and second cathode's pulse, and a longer time between pulses. We used these duty cycles:

- 20 $\mu$s pulse, 30 $\mu$s gap, 640 $\mu$s period (1/32 duty factor)
- 20 $\mu$s pulse, 30 $\mu$s gap, 160 $\mu$s period (1/8 duty factor)

The duty factors listed are for each cathode. In these tests, we were limited by anode outgassing (described later) so we reduced the anode voltage to 10 or 20 kV. Under these conditions, we used cathode currents up to 20 mA (at 1/32) and 4 mA (at 1/8). These duty factors and currents correspond to the final tube requirements.

X-ray generation tests.

To verify the geometry of the multiple x-ray sources that result from the multiple cathodes illuminating the common anode, we constructed a simple x-ray pinhole camera, to give an image of the photon emission from the anode surface. The image was formed on a sheet of high-speed Polaroid film (in a light-tight envelope) mounted below the pinhole. Since the pinhole subtends a very small solid angle, and the Polaroid film is only

moderately sensitive to x rays, this exposure takes a long time. When the Polaroid film is developed in the normal fashion, the bright spots on the film result from the image of the anode regions that emit radiation. The camera is sketched in Figure 5 and an image is shown in Figure 6. With the electron beam at roughly 45° to the vertical, the circular cathode spots project into ellipses around the vertical beam line. These cathodes are spaced by 40.6 mm, and the calculated magnification of the pinhole camera is 0.675; the 29 mm measured spot-to-spot spacing on the film corresponds to a magnification of 0.71. The bright spots are overexposed on the film, so the measurement of their extent on the image (3 mm by 5.5 mm) corresponds roughly to the spot dimensions at 10% of maximum power, rather than at half power. With this measured magnification, the projected (exaggerated) spot size is 4.2 mm by 7.7 mm, produced by a cathode diameter of 5 mm.

Anode thermal tests.

To simulate the bending of the anode in a practical tube, we assembled an experimental copper anode with the same cross section, and heated it with an equally-spaced set of six power resistors on the "front" surface only. This approximates the heating pattern of the discrete set of electron spots from the cathodes. With this experimental system, we could measure the anode bending as a function of anode temperature.

The test anode was supported at two ends, and the deflection was measured with a sensitive dial indicator (1 $\mu$m resolution) at different points along the length. With a 30° C temperature rise of the front surface, we measured a maximum deflection of about 25 $\mu$m for a test anode 30 cm long. (See Figure 7.) This corresponds to the values discussed above in Studies.

We also measured the pressure drop and flow rate for this anode. The measurements are discussed in detail in the Phase II proposal. The measured pressure drop for 1.46 gallons/min of water (sufficient to remove 1.92 kW, or 12 mA at 160 kV, with only 5° C rise) was only 1.4 psi. Using insulating transformer oil instead of water, with different viscosity and heat capacity, we can calculate pressure drops of 14 psi and 3.5 psi for temperature rises of 5° and 10° C, respectively.

# Designs

New circuits have been developed for fast, accurate cathode switching. The logic portions have been prototyped and their circuit diagrams are attached to the end of this report. Figure 8 is a circuit diagram of the cathode switching board. The function and performance of the switching circuit are described below.

A mechanical assembly drawing of our new cathode-grid assembly is shown in Figure 9. This drawing shows a 7.5 mm cathode, but it can be used with any smaller cathode diameter. The important design criteria of this assembly are described below.

## Cathode switch design.

Figure 8 is a slightly simplified schematic diagram of the cathode switch. Since this circuit is an important component of the x-ray source, its operation is described here in detail. The individual cathodes all share a common anode (with a single high-voltage supply) and the individual grids all connect to a single grid bias supply. Each cathode has its own filament transformer (for the heater) and switch board. All switch boards run from a common set of low-voltage (± 15 V) and switching voltage (+ 150 to 200 V) DC supplies.

This circuit switches the cathode terminal for each triode section, with the grid held at a constant voltage. Both the grid bias voltage and the cathode switch are referenced to ground; the anode is held at a constant positive high voltage with respect to ground. Keeping the complex part of the circuit (especially the set of cathode switches) near ground greatly reduces the cost of the system. To obtain a given value of cathode current at the fixed anode voltage, the cathode voltage must be adjusted to get the correct (net) value of grid-cathode voltage. Since the individual grid-cathode assemblies vary slightly in tube parameters, the cathode switch must adjust that voltage automatically. In principle, the switch board could drive the grid and measure the cathode current, but that would put the tube inside the feedback loop, which would be more prone to instability. Our circuit "forces" the cathode current to be

correct. In our experiments, we had extremely long wires (about 20 feet) between the vacuum chamber and the switch boards (outside of the lead-shielded room). Despite these long cathode and grid wires, we still obtained sub-microsecond rise times for the cathode current. In the final system, the boards would be mounted only inches from the tube connection.

A minor disadvantage of switching the cathode instead of the grid is the low insulation rating of the standard heater. This requires a separate filament transformer for each heater, to avoid excessive voltage between the heater and cathode when pulsing the cathode voltage. Cathode assemblies with higher voltage insulation are available, if these transformers are not wanted. The filament transformer in Figure 8 connects to the cathode through resistors, to protect against possible heater-cathode shorts. These resistors are small enough that the common-mode voltage on the transformer winding follows the rise and fall of the cathode voltage waveform, but large enough to minimize the flow of heater current through the cathode wire, should the cathode short to the heater internally.

The operational amplifier U2 and the MOSFET M1 form a voltage-to-current amplifier. The source current of M1, essentially equal to the drain current, flows through the current sense resistor R7. This voltage feeds back to the amplifier's inverting input (pin 2) through feedback resistor R6, and is compared with the input voltage at the amplifier's non-inverting input (pin 3). At equilibrium, these two voltages must be equal. (The output of U2 is finite and the voltage gain of U2 is very high, therefore the voltage difference between pins 2 and 3 will be small.) The voltage reference U3 and CMOS switch U4 produce a waveform that switches between 0 and +5 V (adjustable with RV1). With R7 = 50 Ω, the +5 V level results in a MOSFET current of 100 mA. To change the current set point by a large factor, the value of R7 is changed. To obtain 10 mA, we changed R7 to 500 Ω. We used Caddock non-inductive precision power resistors at R7 for accurate high-speed performance. Since the capacitances of power MOSFETs are rather high, especially the Miller-effect capacitance of the gate-drain junction, we chose an operational amplifier that was optimized to drive capacitive loads.

To guard the circuit against fault conditions, we protected the MOSFET M1 with a spark gap, diode, and fuse. The drain resistor R9, through which the cathode current flows, limits the current into the protection devices. Zener diodes DZ1 and DZ2 limit the

voltage spikes that can hit the operational amplifier. Furthermore, the pulse input to the CMOS switch U4 passes through an optoisolator U1, to eliminate voltage spikes back to the control sequencer and ground loops between the high-power switch board and the lower-power controls.

An optional circuit, built around the high-voltage PNP transistor Q1, gives a useful test point that monitors the cathode current. The circuit senses the actual cathode current (through resistor R9), and does not see the small current through the pull-up resistor R8. The voltage across R9 and D5 appears at the base of Q1, in series with the emitter resistor R10. (Diode D4 provides a path for reverse current.) Since the forward diode drops of D5 and Q1's base approximately cancel, the voltage across R10 equals the voltage across R9, and the current through R10 flows through the transistor Q10 to the load resistor R12. The voltage across R12 is then proportional to the cathode current; since it is referred to ground, it can be measured on an oscilloscope without interfering with the feedback circuit. With the values in Figure 8, the test point output voltage $V_t = I_k$ x (10 Ω) . We verified the calibration of each board's test point with DC meters on the bench before using the board with the tube.

The drain-source voltage rating on the MOSFET is 400 V, but similar devices are available up to 800 V, should higher voltage be necessary. This drain voltage specification limits the board supply voltage $V_{dd}$, which determines the peak-to-peak value of the grid-cathode voltage. When the output of U4 is zero, the MOSFET M1 must shut off. Resistor R8 charges the MOSFET capacitance and pulls up the cathode terminal to $V_{dd}$, to shut off the cathode quickly. The "off" value of the grid-cathode voltage is the difference between the grid bias voltage (positive or negative, as required) and the (positive) supply voltage to the board (+150 V in our experiments).

The feedback circuit adjusts the "on" voltage to obtain the desired current. The minimum voltage on the cathode (tending to increase the current) is the product of the cathode current and the total board resistance. In the circuit shown, set for 100 mA, the resistance is 150 Ω and the minimum voltage is 15 V. With the grid bias set to zero, the grid will always be negative with respect to the cathode, by at least 15 V. If the required "on" value for $V_{gk}$ is less negative than -15 V, then a small

positive grid bias voltage can be used. (However, we recommend using negative net grid-cathode voltages, to avoid grid current.)

To summarize, these considerations determine the grid bias voltage $V_g$ and the switch supply voltage $V_{dd}$: For a desired anode voltage, choose $V_g$ to obtain sufficient cathode current with $V_k$ = +15 V (for the worst-case triode), and then choose $V_{dd}$ to ensure that the most negative $V_{gk} = V_g - V_{dd}$ will be sufficiently negative to cut off the worst-case triode.

In Figure 8, we also show the connections to one cathode of the multiple-source tube. The anode is common to all sections of the tube, and a single grid bias supply connects to every grid in the tube. Each cathode has its own switch board and filament transformer. In the two-cathode experiments, we used a rheostat in series with each transformer, as shown in Figure 8, to control the current individually, but we found that the currents were substantially equal for both heaters. Therefore, in the final system we shall use transformers with primaries in series, to ensure equal currents in all heaters, even with isolated secondaries.

The switching speed is limited by the internal capacitances of the MOSFET, which are much higher than the tube's capacitances. Since the drain voltage swing is large, the Miller effect increases the apparent value of the gate-drain capacitance to several nF, as seen by the output of the operational amplifier. To turn the MOSFET on, the amplifier output current must charge that capacitance to a sufficiently high gate voltage, at which point the MOSFET conducts large currents to charge any other capacitances. When turning the circuit off, the amplifier must supply a similar charge in the opposite direction, but the current to pull the drain positive must be supplied by the pull-up resistor R8, rather than by the large current capability of the MOSFET. The value of the pull-up resistor is a compromise: decreasing R8 (higher current) increases the speed at turn-off, but increases the board's power dissipation and introduces an uncertainty in the actual cathode current, since the current through R8 varies slightly with the voltage at the cathode terminal and is included in the current through the sense resistor R7. For the 100 mA circuit in Figure 8, the current through R8 = 25 kΩ varies between about 4 and 6 mA, depending on the grid-cathode voltage at 100 mA, for an uncertainty of about

1%. With these values, we measured the cathode current rise time (10% to 90%) to be 850 ns, the fall time (90% to 10%) was 450 ns, and the delay time from the pulse input was 620 ns (including the delay of the optocoupler).

A brief report on the measured performance of this design is included in the Appendices.

Cathode-grid assembly design.

We designed a modular cathode-grid assembly for further experiments. This assembly is shown in Figure 9. This assembly can be installed with a minimum cathode-to-cathode spacing of 15 mm, and can be assembled easily before installation in a chamber or tube. To use smaller cathode areas than the 7.5 mm diameter cylinder in this drawing, the cathode vendor (SpectraMat, Inc.) can supply cathodes with the same outside dimensions, but with only a small circle that emits electrons. One such design is shown in Figure 10, where the protruding tip is the only active area of the cathode. This approach would be more robust mechanically than a miniature cathode cylinder for small spot diameters. As a practical matter, we can obtain spot sizes smaller than 1 mm with this approach.

Using such a cathode with the same grid dimensions as these experiments, the cathode current would scale down by the ratio of cathode areas, for equal applied voltages. Since we easily obtained 100 mA for a 5 mm diameter cathode, we conservatively could obtain 10 mA (at 80 kV) with an effective cathode diameter of 1.6 mm. In fact, we extrapolate the data to 10 mA at an effective diameter less than 1.0 mm. This extrapolation assumes that the anode voltage will be 160 kV, which will increase the space-charge limited current at zero bias by a factor between 2 and 3 compared with our 80 kV data, and notes that even at 80 kV, the 100 mA current limit of the switching board occurred at substantial negative bias.

## Failures

One of the cathodes developed a heater-cathode short, inside the cylinder, after several days of operation. We were able to fix this by adding the resistors between the cathode and heater transformer, as described above.

We had several components on the switching board fail during early testing, when we had high-voltage breakdown problems. We located these parts and replaced them with higher-voltage units.

## Difficulties

The experimental vacuum system in this Phase I program was purchased originally on Contract No. DAAK70-88-C-0027 with Fort Belvoir in 1988. When recommissioning this system, we found that a pump and several other items needed replacement, which delayed the start of our experiments. After replacing the pump, we found that our existing anode assembly had a defective seal. Since that ceramic-metal assembly could not be replaced during the time available (the ceramic pieces were not available from stock), we elected to repair the existing system using high-vacuum epoxy, which seriously limited the bake-out temperature of the anode assembly. This did not allow us to "outgas" the anode sufficiently. (In factory-built x-ray tubes, the anode is normally outgassed by induction heating to at least 400° C.) We had to repair the anode seals twice, apparently due to excessive stress on the assembly during routine bakeout. The original ceramic-to-metal seals have sufficient temperature rating, but were apparently broken by an accidental mechanical stress during the earlier project. Our discussions with Richardson Electronics indicate that this epoxy, although needed to stop an intolerable hole in the vacuum seal, is also an outgassing problem. They will help us to outgas our replacement anode properly for further tests that we shall do for our project with Fort Belvoir.

With a "gassy" anode, we encountered excessive pressure rise when

electron current hit the anode. The initial tests were done at low duty factors, so the heat load to the anode was negligible, but at sufficiently high current the pressure would increase above the safe pressure for the cathodes and possibly induce a gas discharge between the anode and cathode. To cope with this problem, we performed our tests with the high voltage on the anode for a few seconds at a time when we ran at high current. We are confident that with a proper outgas procedure for the anode (not limited by the epoxy repairs) that we can avoid this problem in the future. In fact, as we continued our tests on the existing system, we were able to run at progressively higher average currents, apparently due to slow outgassing of the anode.

The 85 kV operating voltage limit of the experimental chamber is due mainly to the commercial high-voltage feedthrough that feeds the anode. For future experiments, we will surround the "air" side of this device with a container of $SF_6$ gas, which has a much higher dielectric strength than air. The 160 kV requirement for the final design is well within the current state of the art; x-ray tubes with ± 225 kV insulation (450 kV total anode-cathode voltage) are available commercially.

## Plan and Completion Dates

The tasks and completion dates are as follows:

| | Task | Completion Date |
|---|---|---|
| 1. | Cathode Design | June 15 |
| 2. | Focusing | May 15 |
| 3. | Final Design Fabrication | November 1 |
| 4. | Spot Position Control | June 15 |
| 5. | Demonstration | November 30 |
| 6. | Phase II Plan<br>Report | September 28<br>January 5 |

Task 4 became unnecessary when the decision was made to use discrete spots, rather than a continuous sweep. The Final Report in Task 6 concludes Phase I of this project; the Phase II Plan was included in the SBIR Phase II project proposal, which was submitted on September 28, 1995.

## Conclusions

Phase I of this project proved that we can pulse multiple small x-ray sources, each source being defined by a thermionic cathode and control grid. We demonstrated current densities and switching times better than required for the cargo inspection requirement.

This work was based on our experience in the previous "Hydra" x-

ray source project. While the vacuum system came from that earlier project, the switching circuits developed in this work are faster, substantially more stable, and cheaper than those in Hydra.

Since the Phase II proposal was submitted in September, we completed this experimental demonstratation with a laboratory system. The remaining requirements for a practical x-ray source, as described in the Phase II proposal, are to take this experimental work and to design and manufacture the actual x-ray tubes. The remaining design problems are well within the state of the art, and have been solved in the manufacture of conventional x-ray tubes. The novelty here is the use of a compact cathode-grid structure and low switching voltages to control the x-ray beam quickly and efficiently. This method was validated in the Phase I project.

We have discussed the proposed Phase II design with Richardson Electronics, with whom we have worked closely in related x-ray projects. They can readily manufacture this design with ceramic-metal construction, and can assist us with the next development phase.

As the result of the work completed since the Phase II proposal was submitted in September, we can raise the level of assurance that the Phase II development and subsequent Phase III commercialization will succeed.

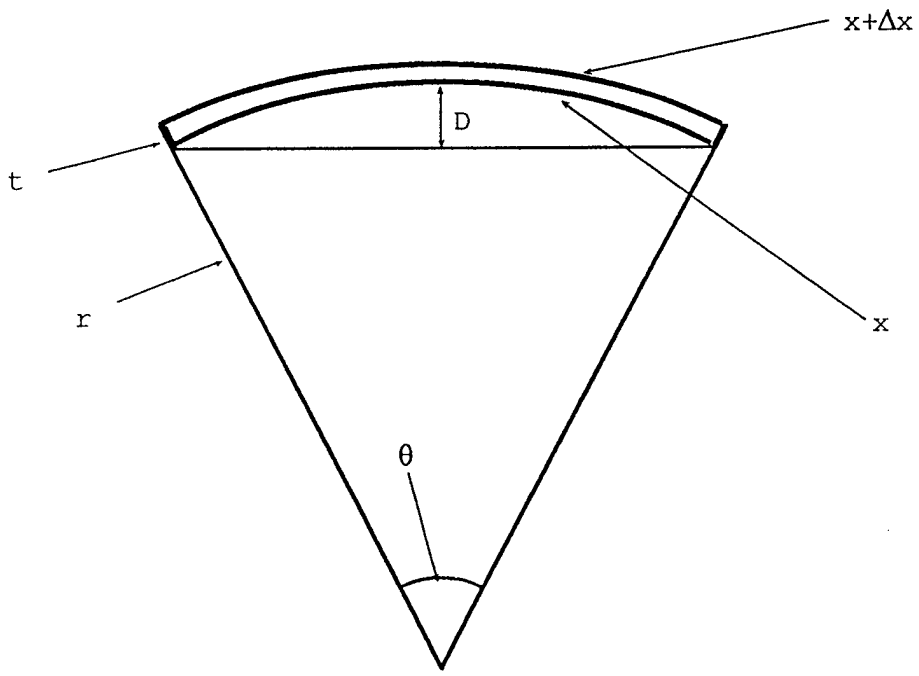


*Figure 1. Geometry of anode deflection calculation.*

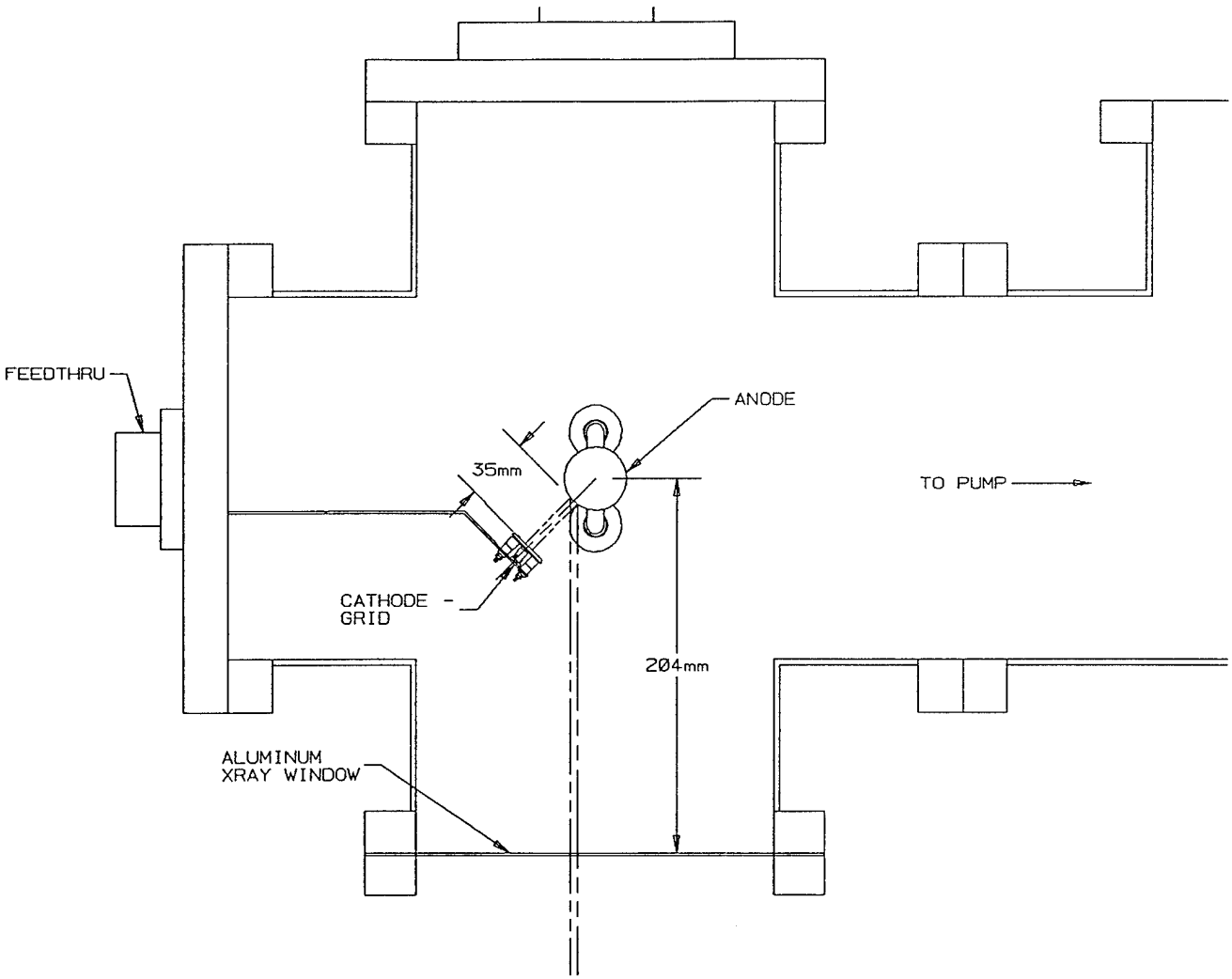


*Figure 2. Cross-section of experimental x-ray tube.*

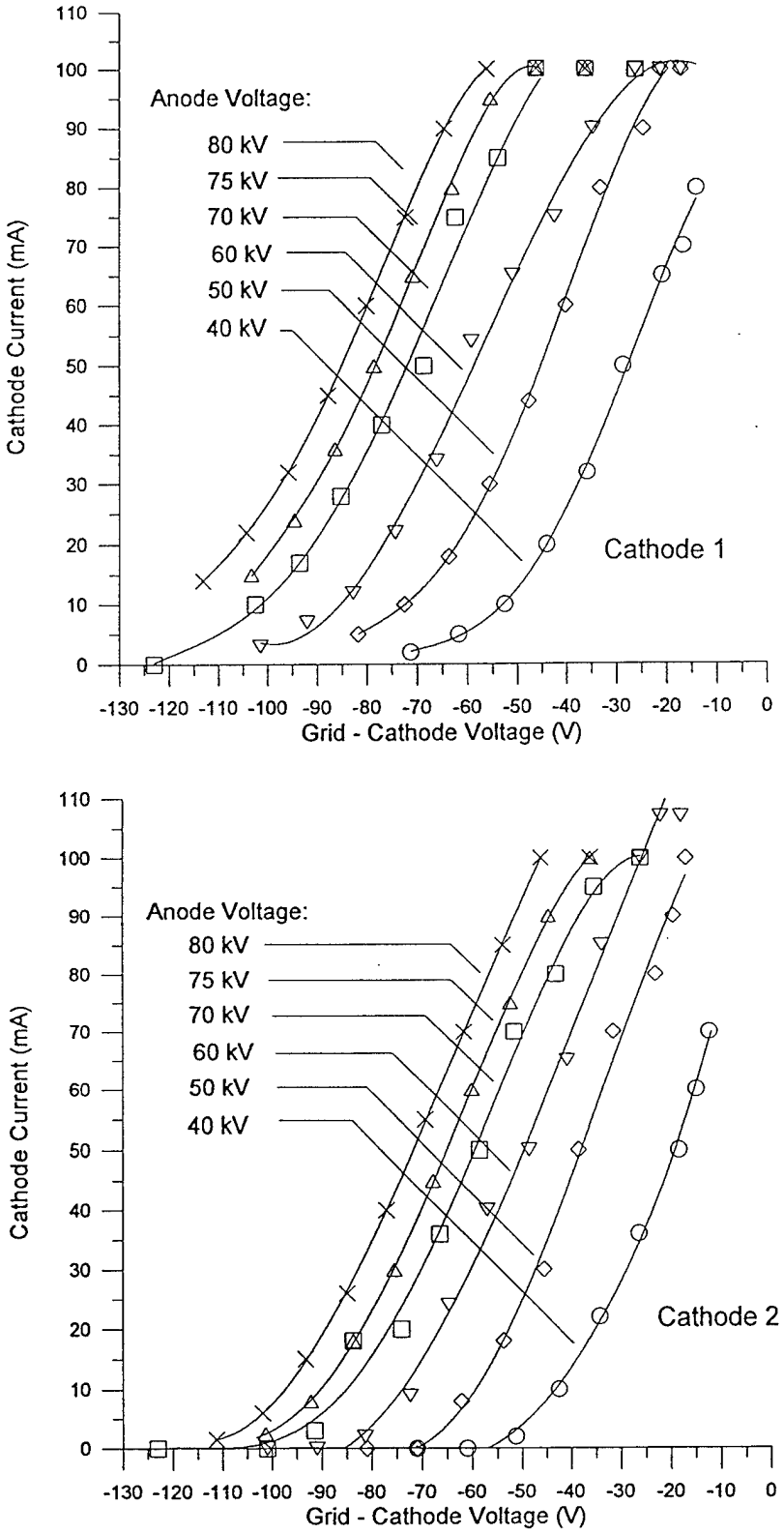


*Figure 3. Measured cathode current versus anode voltage and grid-cathode voltage for two 5 mm cathodes and common anode.*

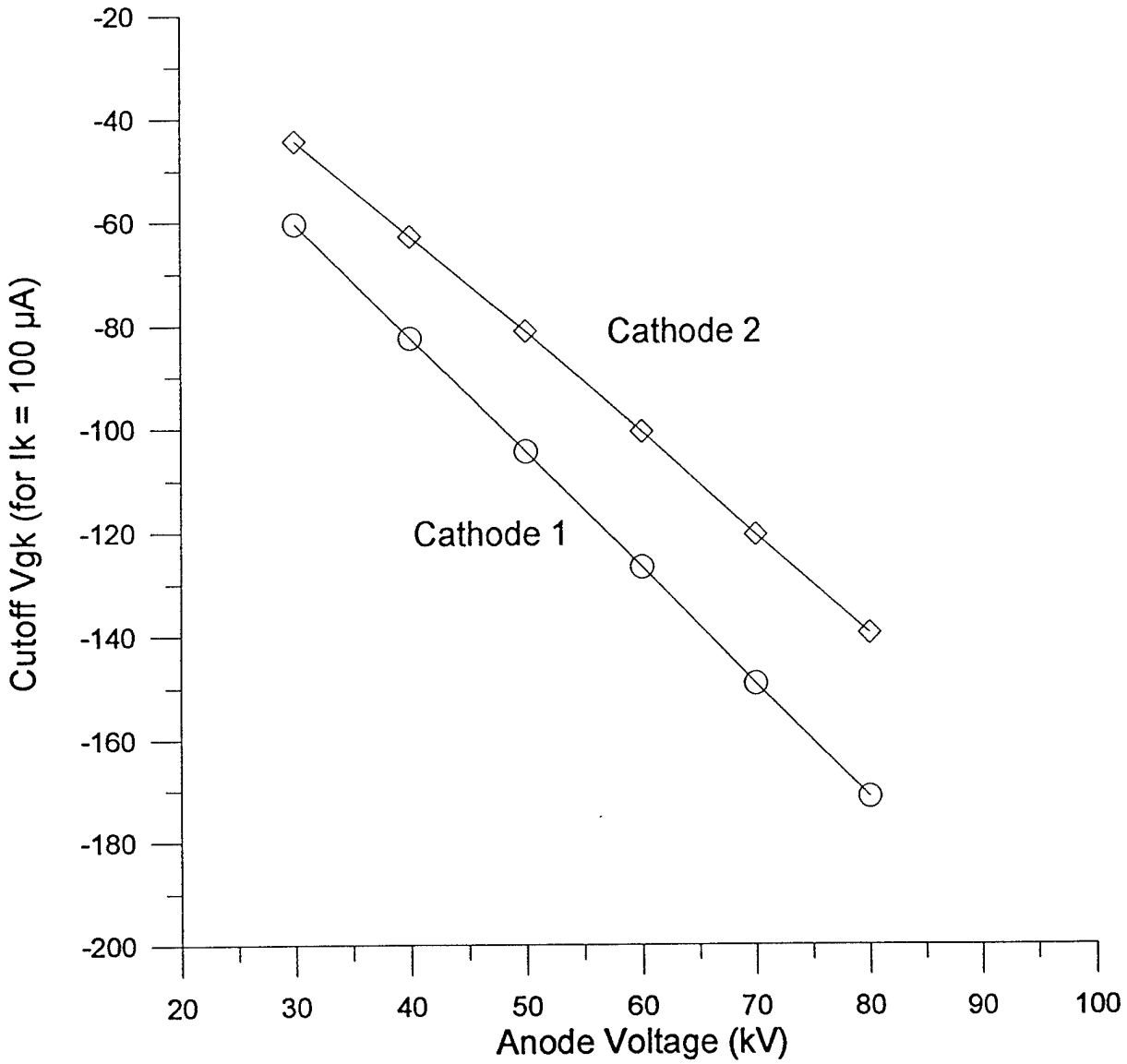


*Figure 4. Measured cut-off grid-cathode voltage versus anode voltage for two 5 mm cathodes and common anode.*

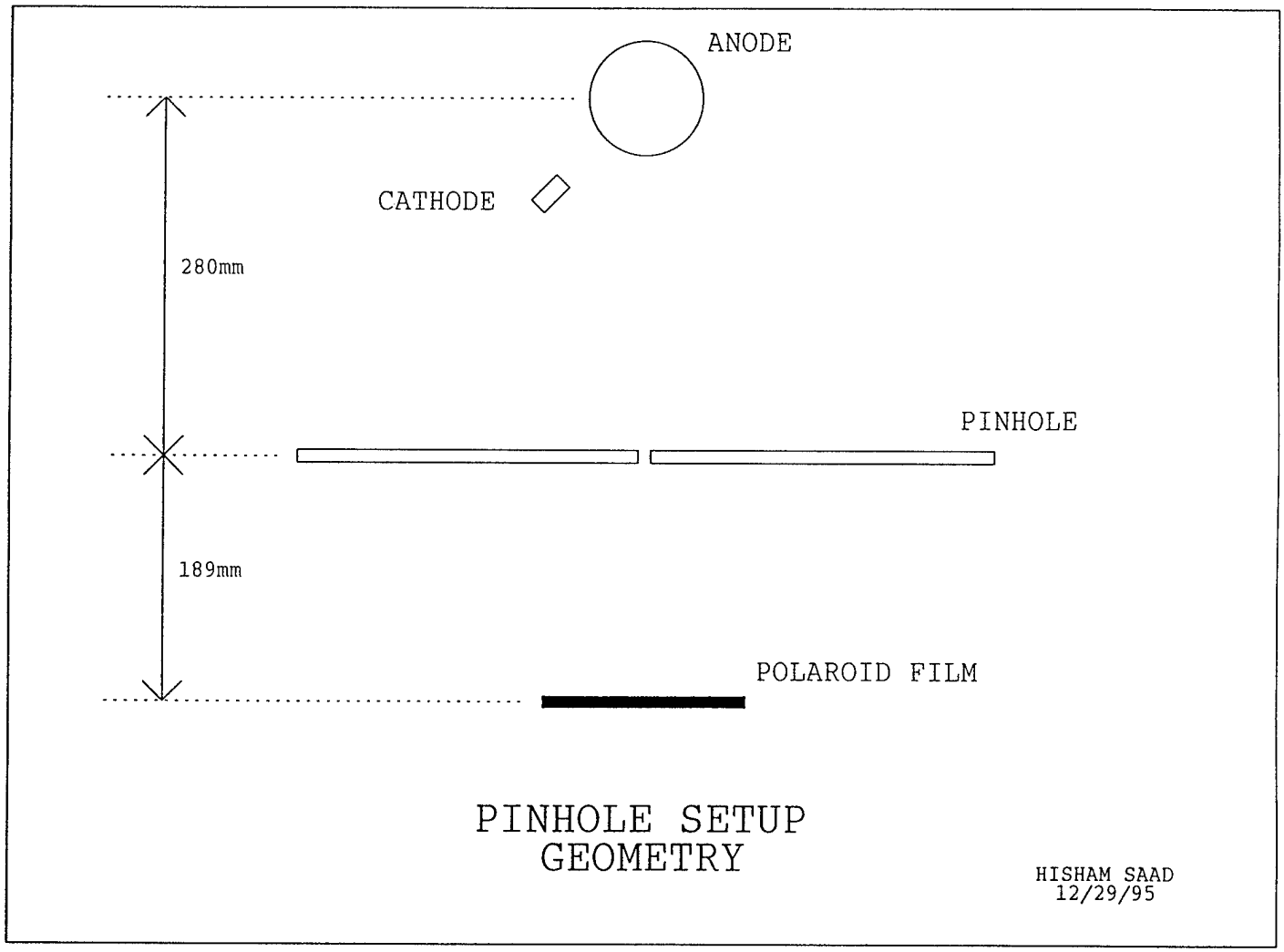


*Figure 5. Geometry of x-ray pinhole camera.*

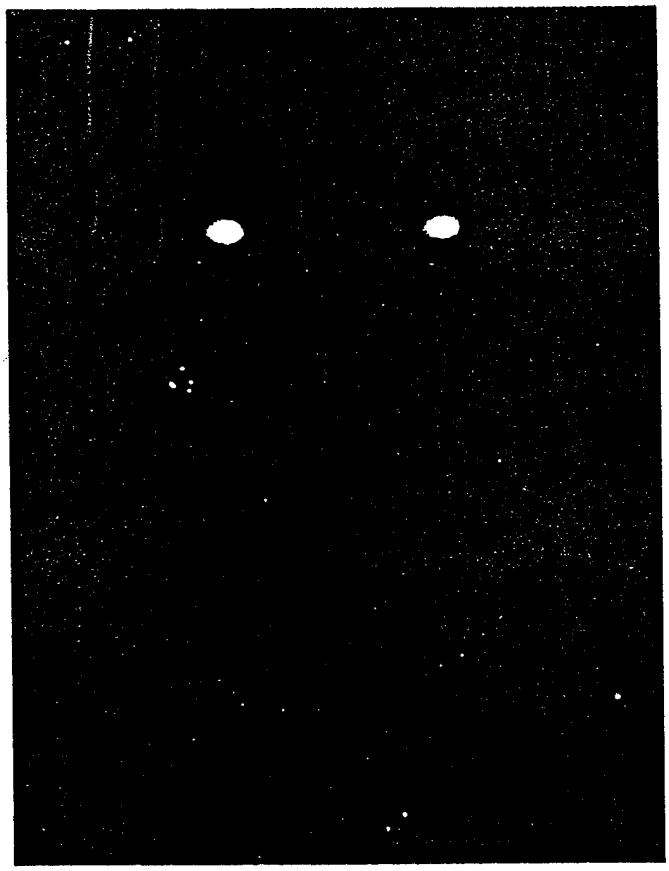

Figure 6. *Polaroid® image of two pulsing x-ray sources taken with pinhole camera.*

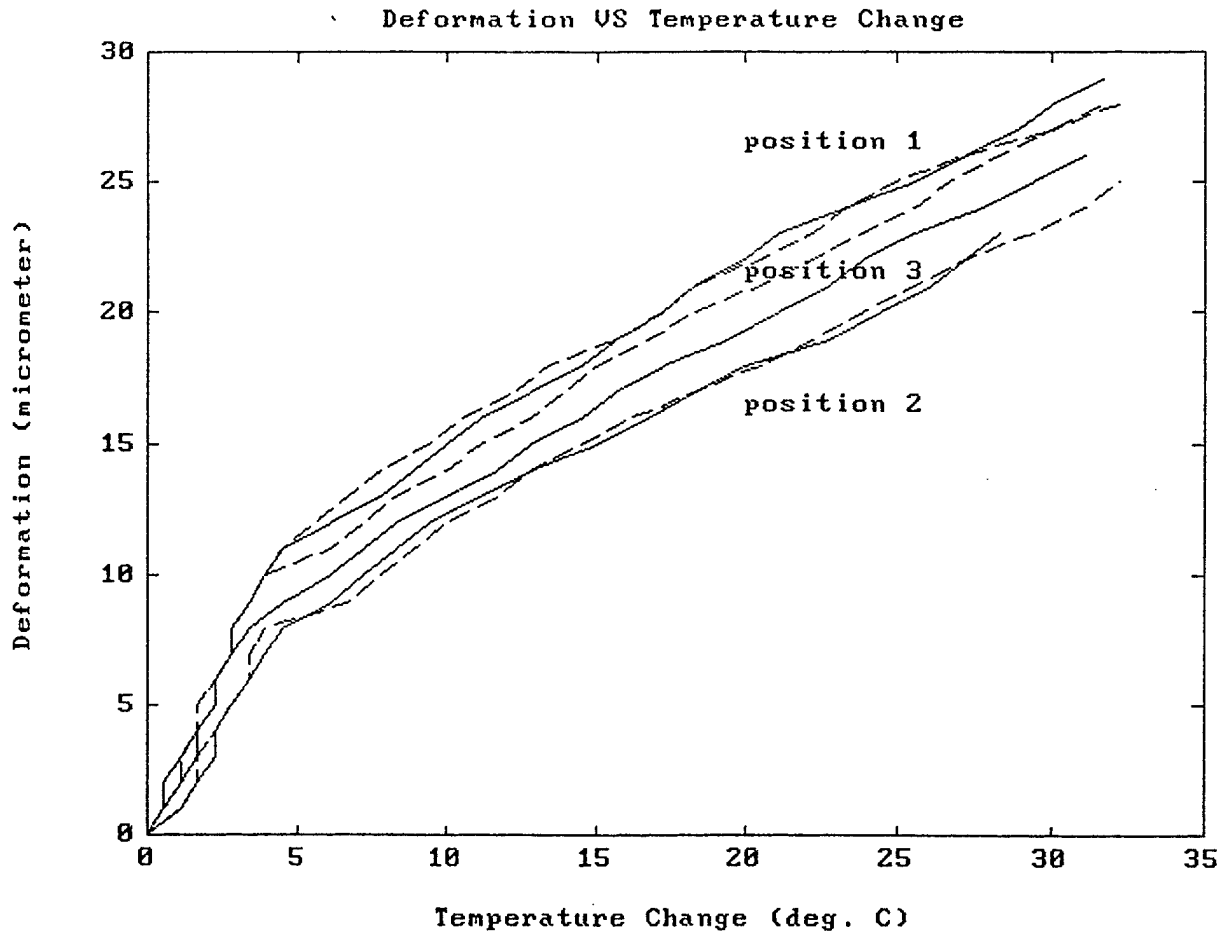


*Figure 7. Measured deformation of experimental anode versus temperature rise.*

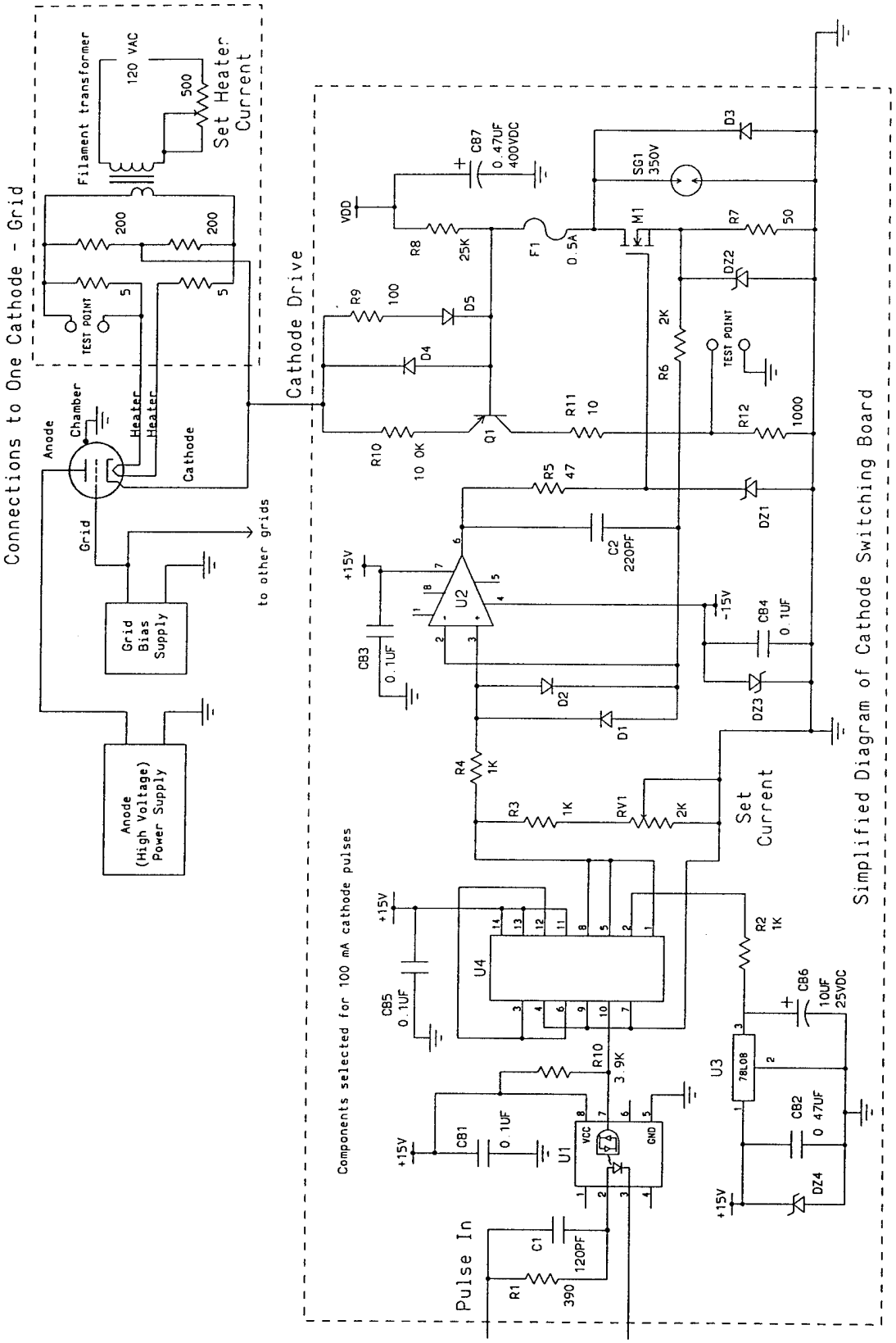


*Figure 8. Circuit diagram of cathode switching board and connections to x-ray tube.*

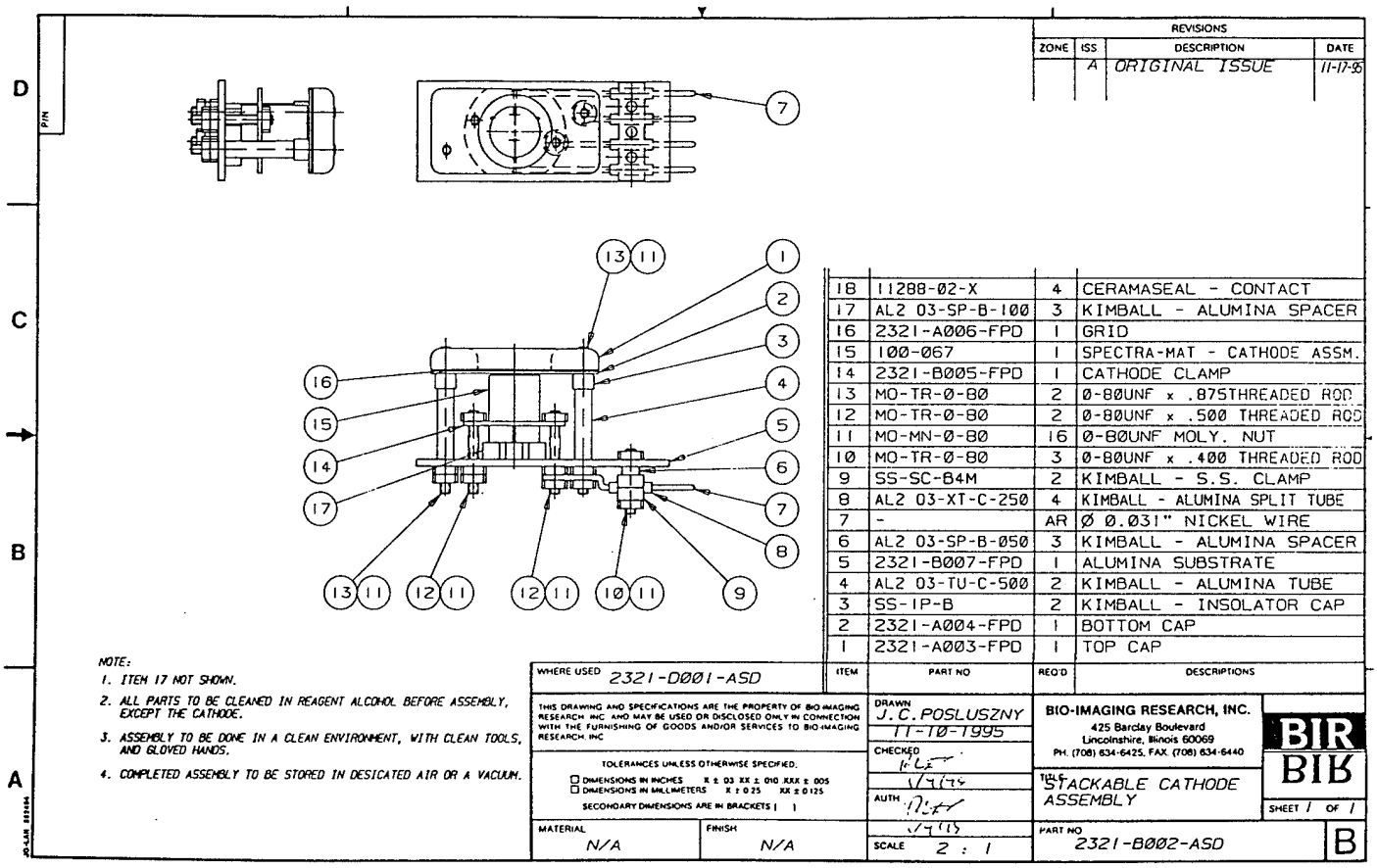


*Figure 9. Design drawing of demountable cathode-grid assembly.*

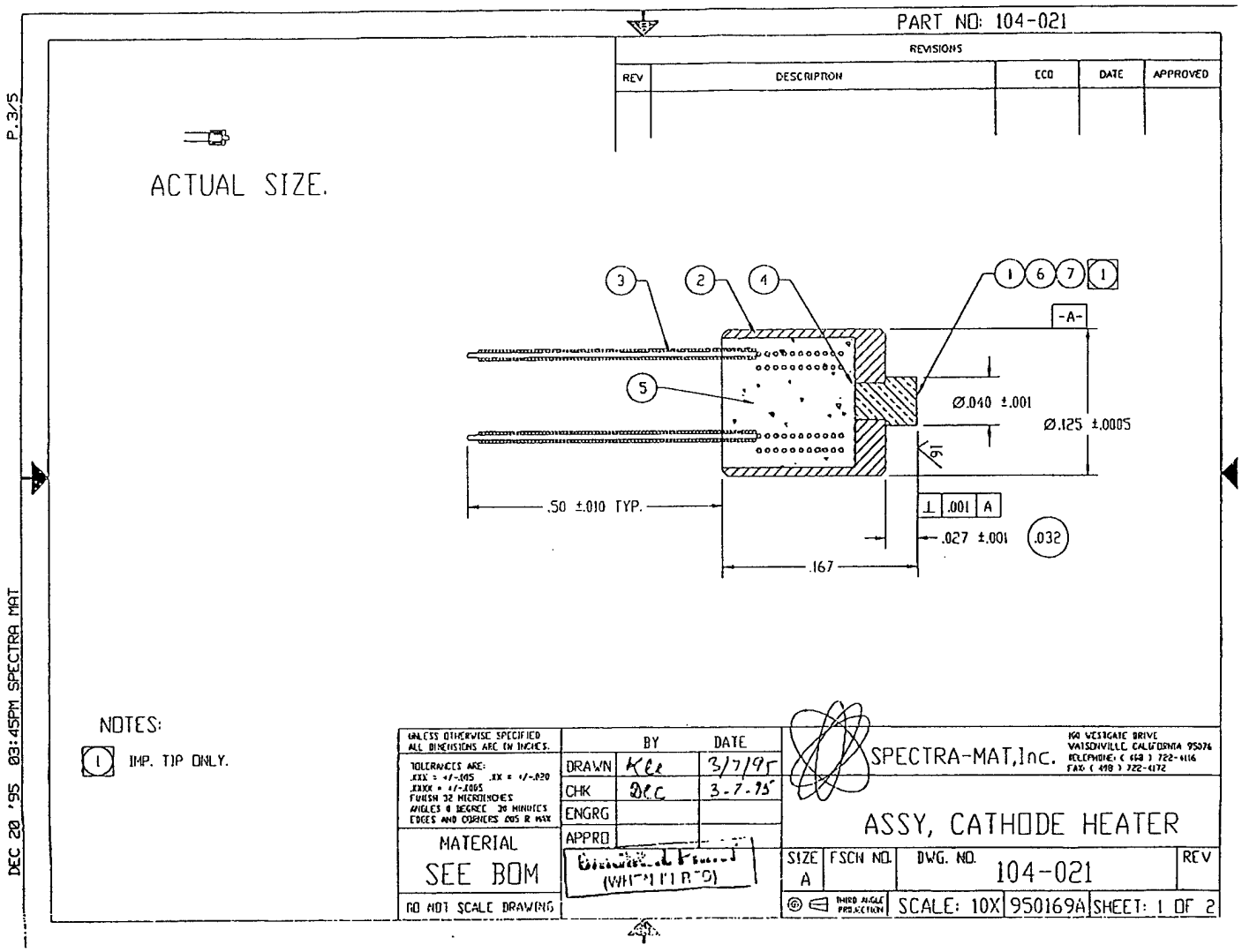


*Figure 10. Example of commercially available reduced-area cathode assembly (from Spectra-Mat, Inc.).*

| PARAMETER | Band A | Band B | Band C | Band D | Band E | Total |
|---|---|---|---|---|---|---|
| | | | | | | |
| Band limits | 0 to 55 kV | 55 to 69 kV | 69 to 95 kV | 95 to 115 kV | 115 - 160kV | |
| | | | | | | |
| Photons/sec-sqmm-mA, in Air | 4.98E+06 | 3.70E+06 | 1.96E+06 | 1.02E+06 | 8.40E+05 | 1.25E+07 |
| Photon rate, 20cm H2O | 27400 | 57400 | 48800 | 34200 | 40200 | 208000 |
| | | | | | | |
| Photon rate, with 5M/sec limit, Air | 1.99E+06 | 1.48E+06 | 7.84E+05 | 4.08E+05 | 3.36E+05 | 5.00E+06 |
| Photon rate, 5M/s limit, 20cm H2O | 10960 | 22960 | 19520 | 13680 | 16080 | 83200 |
| Photon count in 1/60sec, 20cm H2O | 183 | 383 | 325 | 228 | 268 | 1387 |
| | | | | | | |
| Attenuation through 20cm H2O | 181.75 | 64.46 | 40.16 | 29.82 | 20.90 | 60.10 |
| Attenuation coefficient, sqcm/gm | 0.260 | 0.208 | 0.185 | 0.170 | 0.152 | 0.205 |
| Energy corresponding to coefficient | 48 kV | 61 kV | 80 kV | 102 kV | 145 kV | |
| | | | | | | |
| CdTe absorption at above energy | 100.0% | 100.0% | 97.6% | 87.3% | 53.5% | |
| Detected photons, 1sqmm, 1/60sec | 183 | 383 | 318 | 199 | 143 | 1225 |
| | | | | | | |
| Detected photons, 4sqmm, 1/60sec | 731 | 1531 | 1270 | 796 | 574 | 4901 |

*Table 1. Tabulated results of required photon rate for scanner.*

## APPENDIX 1

Photographs of Experimental System

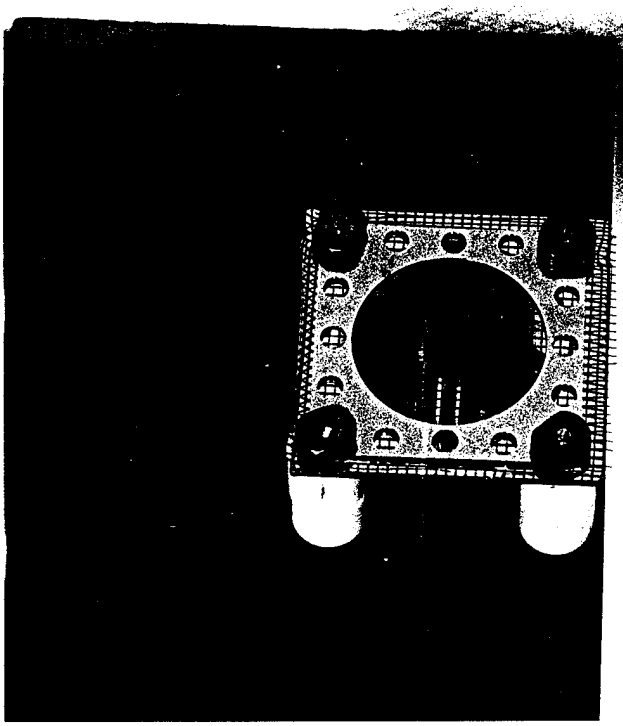

*Single cathode with original grid frame, used in first tests.*

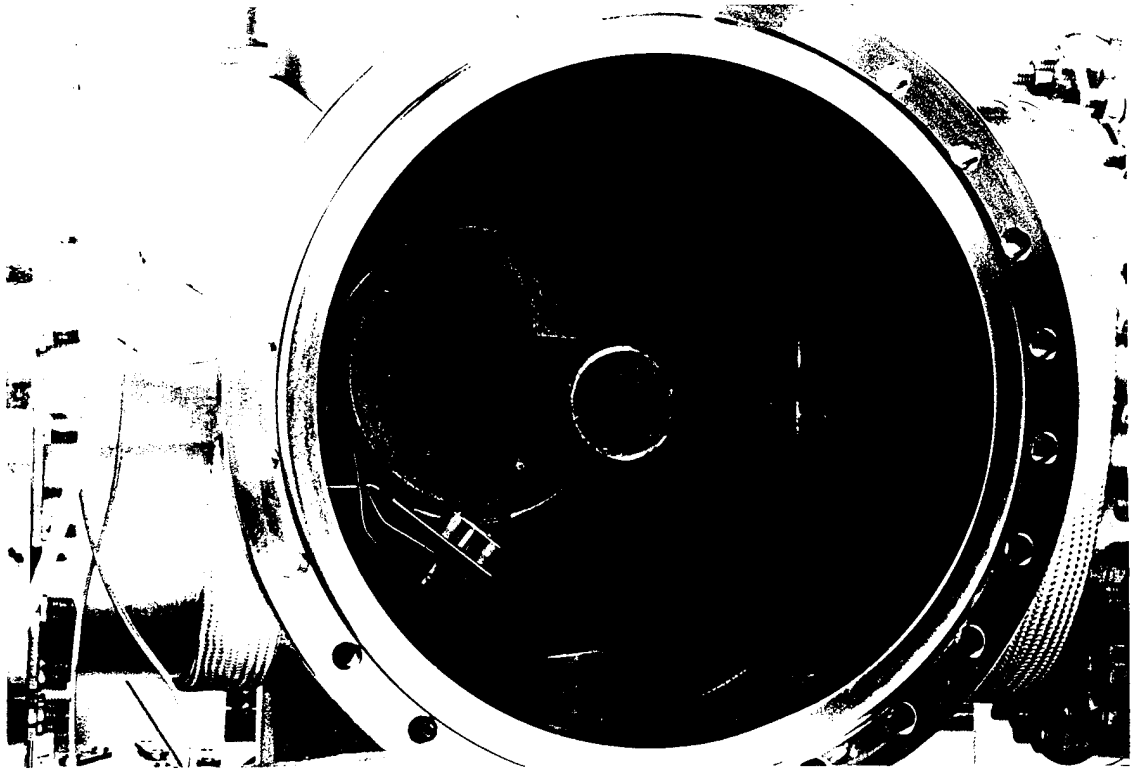

*View into vacuum chamber showing single cathode-grid assembly and long cylindrical anode.*

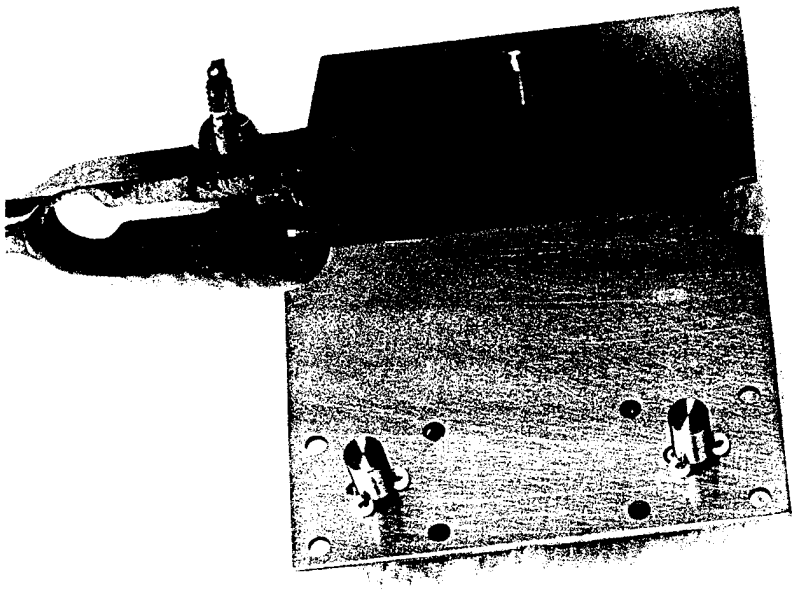

*Two cathodes, without grids, mounted on molybdenum plate.*

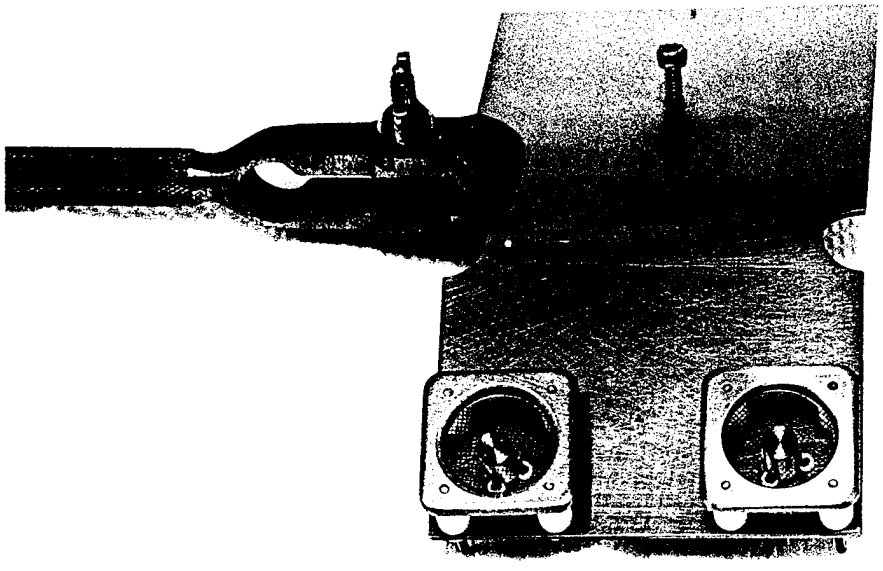

*Two cathodes with improved grid frames.*

# APPENDIX 2

Hisham Saad
12/29/95

## High Voltage Switching Board
## Measured Performance Summary

Operation of the switching boards when connected to the X-ray tube:

1. Difference between 10mA and 100mA PC board schematics:

| | 10mA board | 100mA board |
|---|---|---|
| R7 | 500Ω | 50Ω |
| R8 | 150kΩ | 25kΩ |
| R9 | 1kΩ | 100Ω |
| R10 | 100kΩ | 10kΩ |
| R12 | 10kΩ | 1kΩ |

2. a. The rise and fall time of the waveform measured with the current probe at the cathode pin of the 10mA board are 200nsec and 3μsec respectively.

   b. The delay between the signal measured at the pulse generator output and the signal measured with the current probe at the cathode pin of the 10ma board is 1.6μsec for the rising edge and 2.4μsec for the falling edge.

   Note that there are long wires connecting the board and the X-ray tube.

3. The test point on the switching board gives a good cathode current pulse amplitude measurement. However, it does not yield a very good indication of the pulse rise and fall time. This problem can be improved by adding capacitance in the test point circuit.

4. The rise and fall time of the waveform measured with the current probe at the cathode pin of the 100mA board were less than 2μsec. Keeping in mind that the board is connected to the X-ray tube through long wires.

Operation of the switching boards when connected to a dummy load (diode in series with a resistor):

5. Difference between 10mA and 100mA PC board schematics:

| | 10mA board | 100mA board |
|---|---|---|
| R7 | 500Ω | 50Ω |
| R8 | 150kΩ | 25kΩ |
| R9 | 1kΩ | 100Ω |
| R10 | 100kΩ | 10kΩ |
| R12 | 10kΩ | 1kΩ |
| Dummy load (resistor) | 2140Ω | 560Ω |

6. a. The rise and fall time of the waveform measured with the current probe at the 2140Ω resistor of the 10mA board are 640nsec and 1.5μsec respectively.

   b. The delay between the signal measured at the pulse generator output and the signal measured with the current probe at the 2140Ω resistor of the 10ma board is 2.2μsec for the rising edge and 1μsec for the falling edge.

7. a. The rise and fall time of the waveform measured with the current probe at the 560Ω resistor of the 100mA board are 1040nsec and 500nsec respectively.

   b. The delay between the signal measured at the pulse generator output and the signal measured with the current probe at the 560Ω resistor of the 100ma board is 630nsec for both the rising edge and the falling edge.

8. Calibration tests were done on the 10mA and the 100mA boards using dc voltages. The following results were obtained.

   a. By varying the simulated cathode voltage, for the 10mA board, from 97.4v to 8.7v (feedback is lost at 15.6v), the ratio between the current through the dummy load (measured with an ammeter) and the voltage at the test point changed by 0.59%.

   b. By varying the simulated cathode voltage, for the 100mA board, from 60.2v to 11.2v (feedback is lost at 16.4v), the ratio between the current through the dummy load (measured with an ammeter) and the voltage at the test point changed by 0.86%.

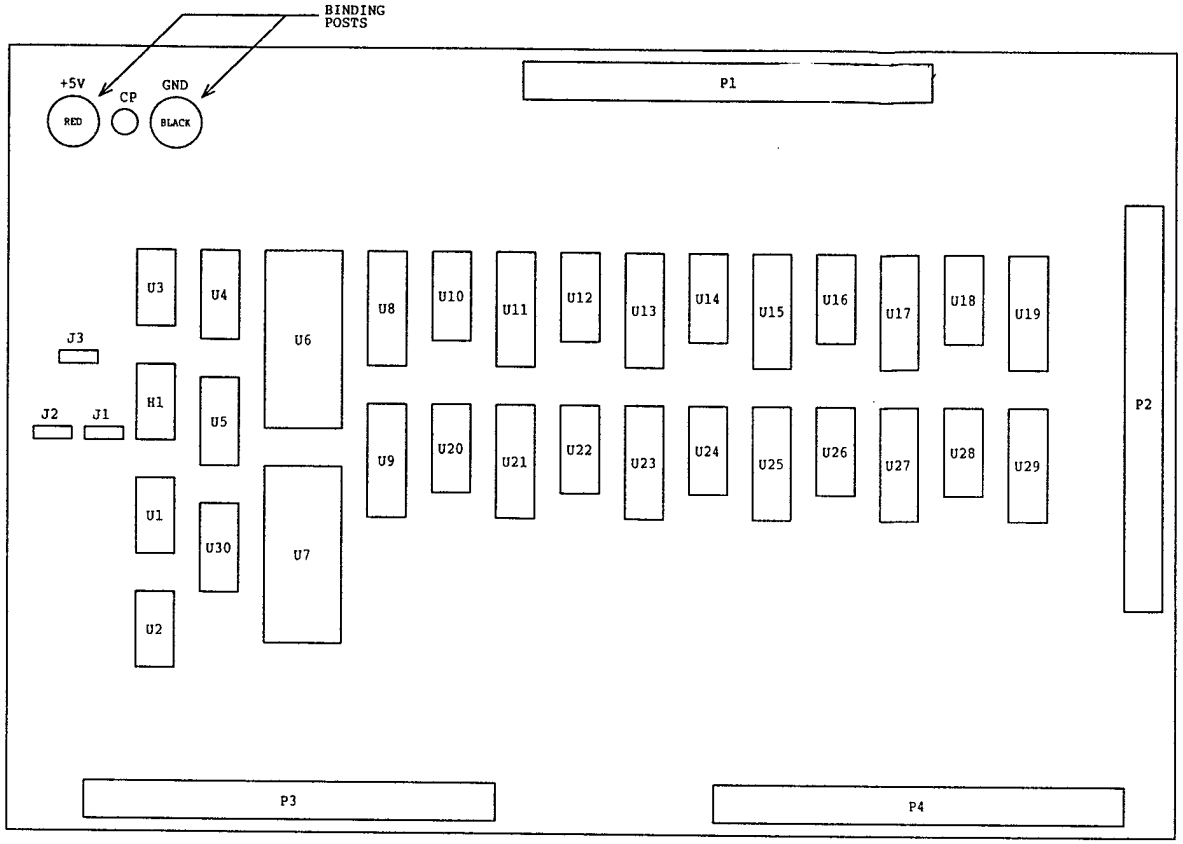


NOTES:

1. IC SOCKETS ARE THE SOLDER TYPE WITH BUILT IN 0.1UF BYPASS CAPACITORS.
2. CP IS 33UF, 35VDC BYPASS CAPACITOR.
3. J1, J2 AND J3 ARE JUMPERS.
4. USE #18 WIRE GAUGE FOR ALL POWER SUPPLY CONNECTIONS.
5. P1, P2, P3 AND P4 ARE 50 PIN HEADERS. CONNECT EVEN PIN NUMBERS 2 THROUGH 50 (OF EACH HEADER) TO GROUND.

ENC_IF.SCH

HISHAM SAAD

5-11-95

CATHODE SEQUENCER BOARD LAYOUT

B

TITLE:

UMD - PHASE II

01

PART NO.

NONE

B

## APPENDIX 3

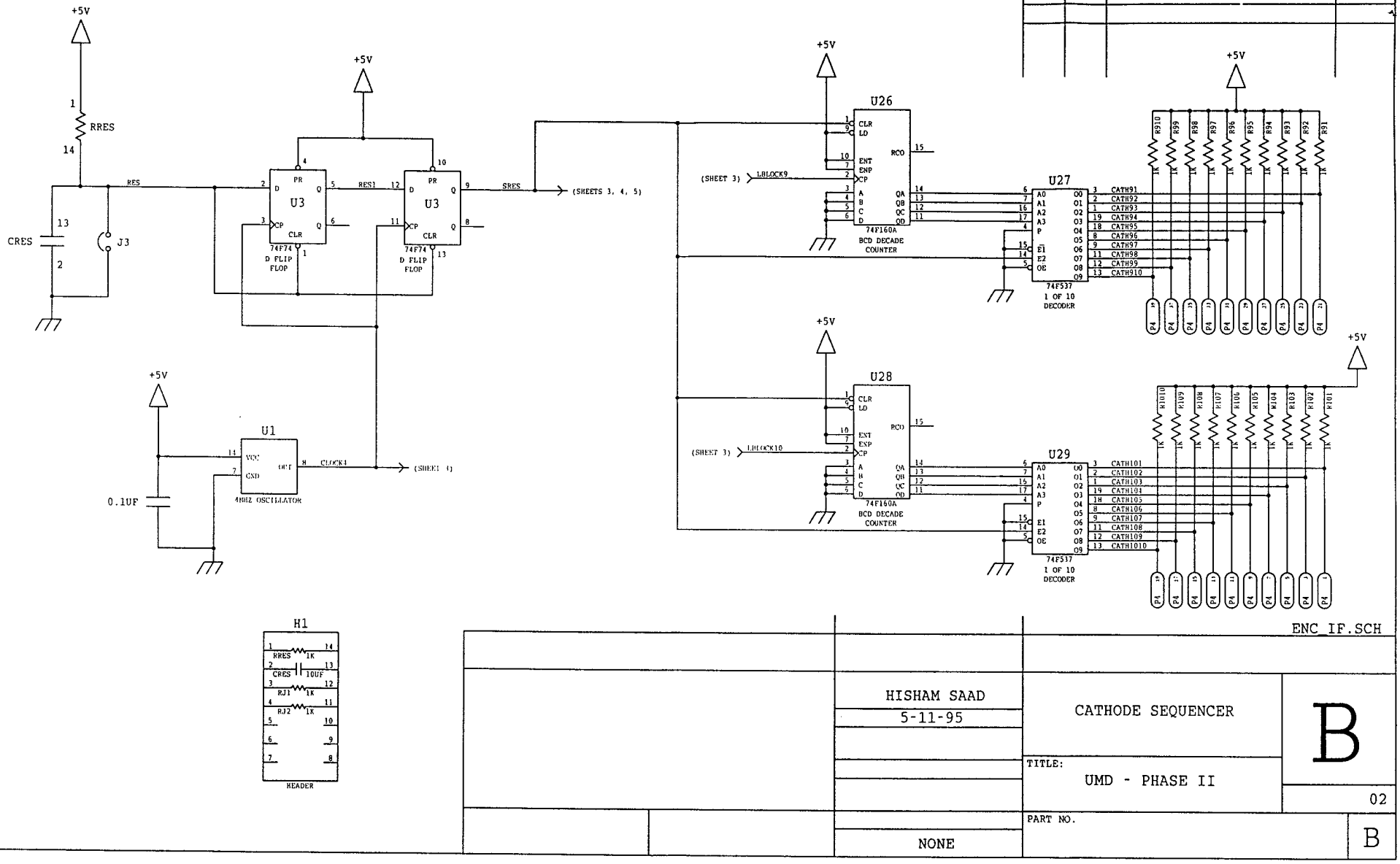


ENC_IF.SCH

| | | |
|---|---|---|
| HISHAM SAAD | CATHODE SEQUENCER | B |
| 5-11-95 | TITLE: UMD - PHASE II | 02 |
| NONE | PART NO. | B |

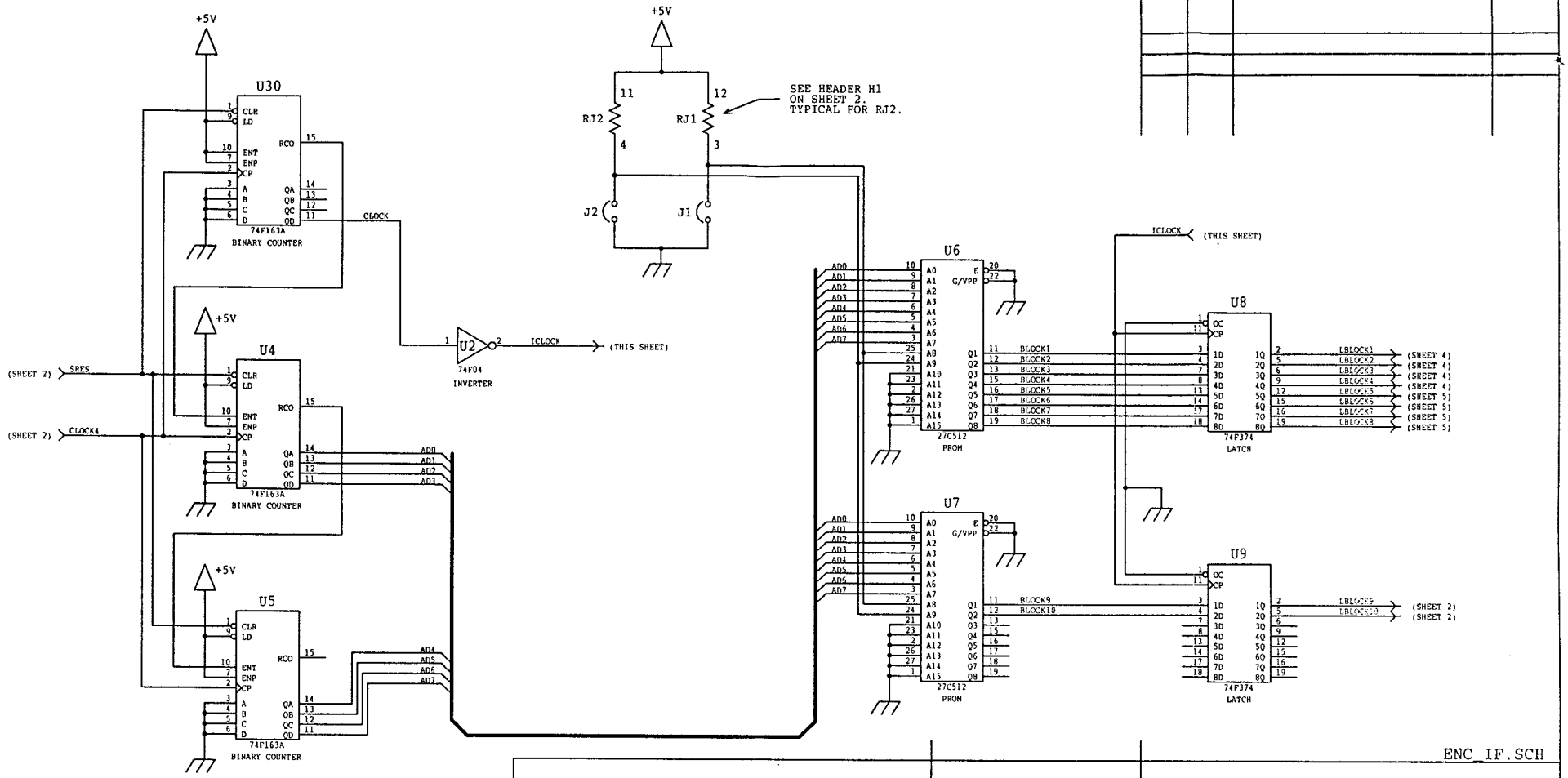


ENC_IF.SCH

| | | |
|---|---|---|
| HISHAM SAAD<br>5-11-95 | CATHODE SEQUENCER | B |
| | TITLE:<br>UMD - PHASE II | 03 |
| NONE | PART NO. | B |

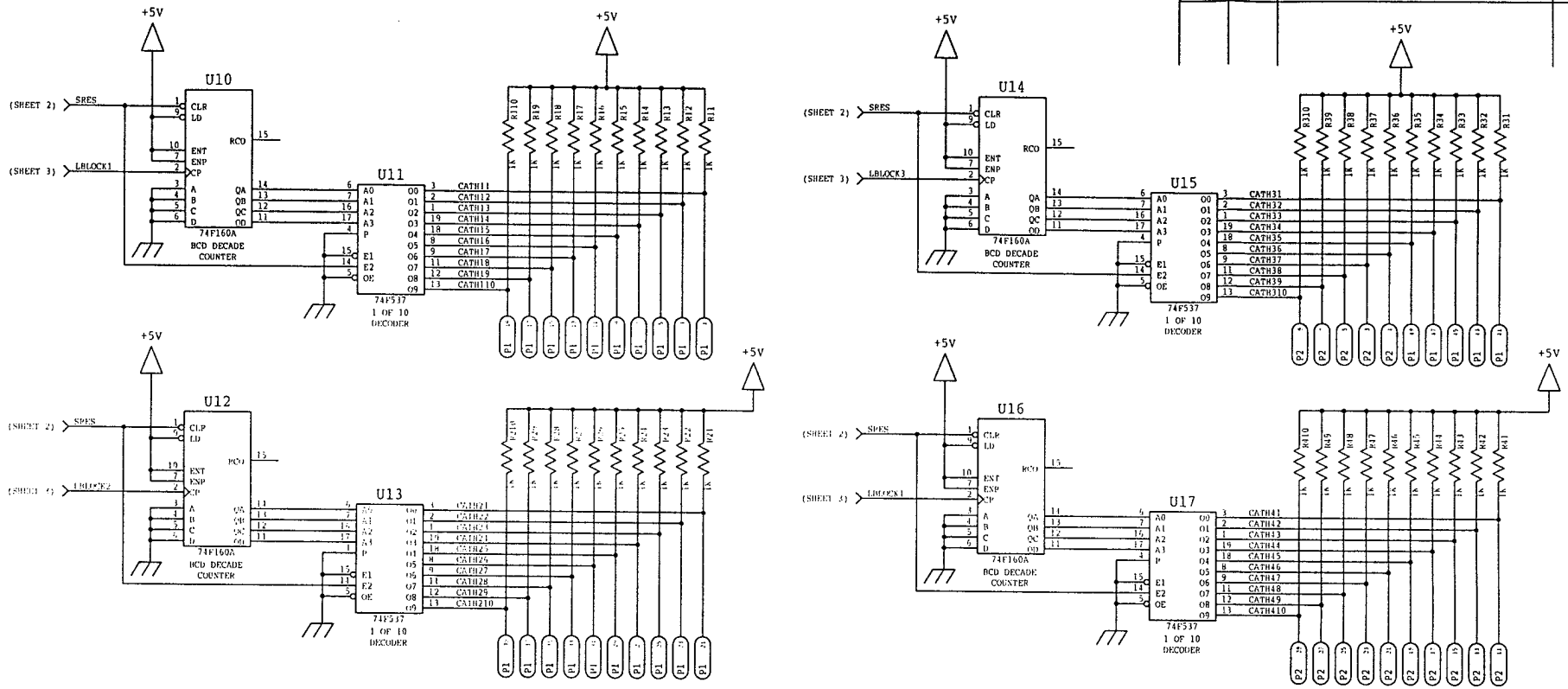


ENC_IF.SCH

| | | |
|---|---|---|
| HISHAM SAAD<br>5-11-95 | CATHODE SEQUENCER | B |
| | TITLE:<br>UMD - PHASE II | 04 |
| NONE | PART NO. | B |

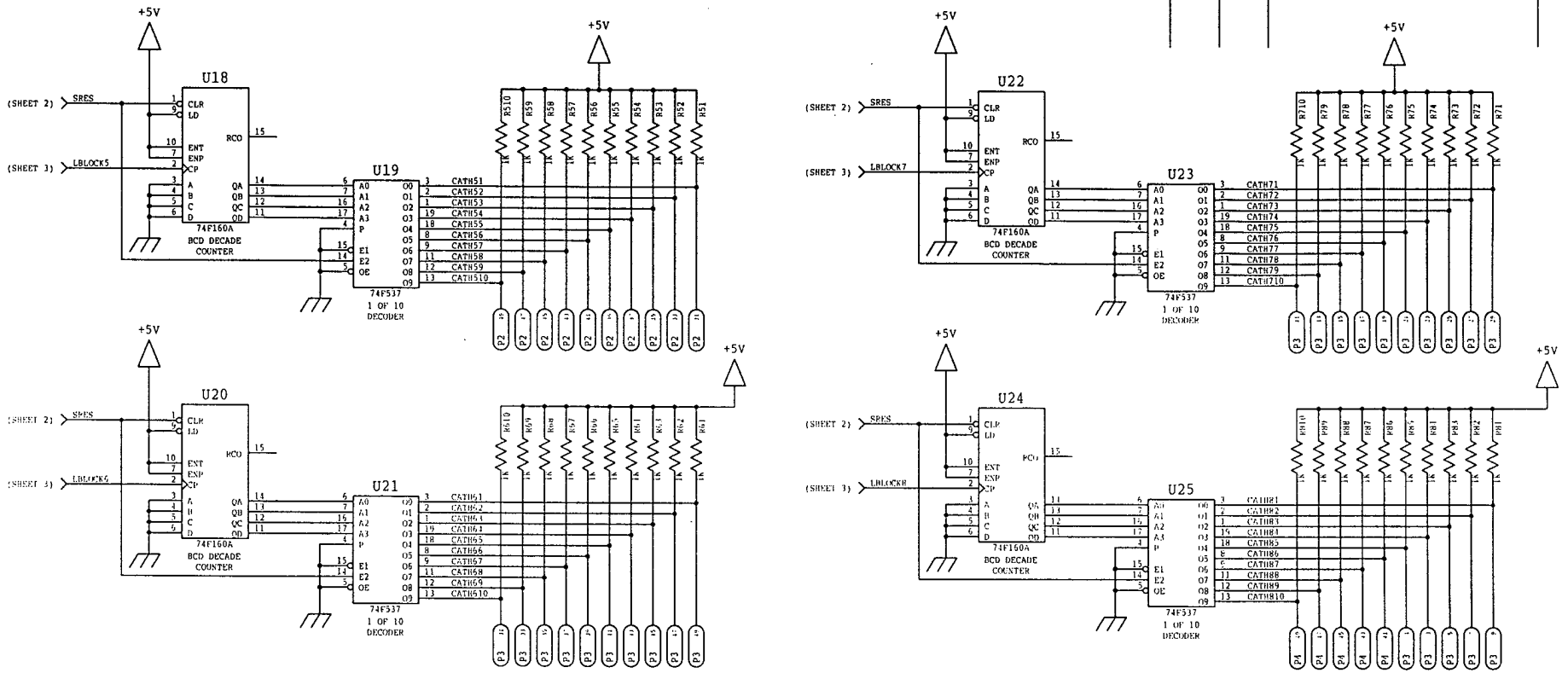


ENC_IF.SCH

| | | |
|---|---|---|
| HISHAM SAAD | CATHODE SEQUENCER | B |
| 5-11-95 | TITLE: UMD - PHASE II | 05 |
| NONE | PART NO. | B |